Materials for life science

Arginine–malate-based dual-emission carbon dots for uric acid determination in human serum with a miniaturized device

Xiaoqiu Gan[1], Elvi Angelina[2], Fangyuan Gu[1], Kewen Zheng[1,*], and Lei Cui[2,*]

[1] *School of Environmental and Chemical Engineering, Shanghai University, Shanghai 200444, China*
[2] *College of Science, Shanghai University, Shanghai 200444, China*

ABSTRACT

Determination of uric acid is very important for the clinical diagnosis of several diseases correlated with their variations in human serum. In this work, dual-emission arginine carbon dots (Arg-CDs) were synthesized for the determination of uric acid (UA). After optimization, the obtained Arg-CD was excited at 360 nm, which exhibited dual-emission fluorescence peaks at 445 nm and 514 nm, respectively. Because of the electrostatic interaction between the secondary amine group in UA and the carboxyl group on the Arg-CD, the formation of hydrogen bonds between the ketone/hydroxyl group in the UA molecule and the amino group on the surface of Arg-CD, the mixture could cause the fluorescent signal to be activated. Particularly, Arg-CD showed a good line relationship to UA between 330 and 630 μM (the concentration of uric acid in the serum for healthy people is 240–520 μM), and the lower detection limits are 7.14 μM. With the high selectivity and sensitivity to uric acid, Arg-CD could be applied in the UA determination of the human serum samples, whose accuracy rate was in the range of 98.5–101.5% and relative standard deviation (RSD) value was lower than 4%. And we also designed a miniaturized device for UA determination conveniently.

Introduction

In living organisms, uric acid (2,6,8-trihydroxy-purine, UA), the final metabolite of purines, is maintained in a dynamic equilibrium in free and bound forms of the human body. In human urine and blood, the amount of uric acid is an extremely important indicator [1]. When the production and excretion of uric acid are unbalanced, metabolic oxidation of the purine base will result in kidney

---

damage, leukemia, hypertension, diabetes, and hyperuricemia [2]. In recent years, the number of patients with hyperuricemia has been rising and becoming more prevalent in younger populations [3]. Therefore, the determination of uric acid with convenience and accuracy is strategic in clinical examination [4]. Although various analytical techniques have been developed in the past few years, such as spectroscopy (ultraviolet absorption fluorescence [5]), electrochemistry (voltammetry [6]), chromatography [7], light scattering [8], enzyme analysis [9], flow injection chemiluminescence [10], and isotope dilution mass spectrometry[11], most of these methods are complex and time-consuming and often require special instruments; thus, a precise and efficient method for UA determination is still urgently needed.

Carbon dots (CDs) are a type of new material with a size of less than 10 nm, which stand out in the carbon family, with their special quantum size effect, and are characterized by abundant surface functional groups, uniform dispersion, tunable composition, good biocompatibility, photoluminescence, etc. [12]. Compared with traditional organic fluorescent dyes, carbon dots combine the attractive properties of biocompatibility, photostability, low toxicity, strong chemical inertness, and adjustable composition [13, 14]. For these reasons, CDs have been broadly applied in cell imaging [15], disease diagnosis [16], drug delivery [17], and electrochemical analysis [18]. Dual-emission fluorescent probes were very promising for the highly selective determination of analytes, which became more appropriate for qualitative or quantitative analysis in comparison with single-emission fluorescent sensors [19]. Studies have been reported about the dual-emission CDs for UA determination, which was less susceptible to hindrance in samples and could be more sensitive and selective for UA.

Nitrogen-doped carbon dots had nitrogen-containing functions and surface defects, which could significantly improve photoluminescence properties [20]. Chen et al. [21] synthesized arginine-modified carbon dots with strong luminescence that could be used for cell imaging under a common fluorescence microscope due to the high cellular uptake efficiency. Zhao et al. [22] reported environment-friendly green-emitting carbon dots for sweat latent fingerprints, which were prepared with DL-malic acid and ethylenediamine. DL-malic acid, as the green and

inexpensive reagent, possesses a hydroxyl group and two carboxyl groups, and these may render its ideal molecular precursor for CDs [23].

Herein, we report a facile strategy to prepare dual-emission fluorescence carbon dots (Arg-CD); L-arginine and DL-malic acid were chosen as carbon and nitrogen sources through the solvothermal method. Arg-CD-based optical carbon dots increase the fluorescence intensity considerably, thereby achieving rapid and sensitive determination of uric acid. The proposed determination strategy is shown in Scheme 1.

Experimental

### Materials and instruments

The materials and instruments used for the study are illustrated in Electronic Supporting Information (ESI).

Synthesis of Arg-CD

A simple solvothermal method was used to synthesize Arg-CD under the heating conditions without complicated chemical coupling modification. As shown in Scheme 1, L-arginine (1.95 g, 11.19 mmol) and DL-malic acid (1 g, 7.46 mmol) were dissolved into the deionized water and ultrasonic for 5 min. Then, the mixtures were transferred into a 25-mL polytetrafluoroethylene-lined autoclave and heated at 195 °C for 2 h. The reaction solution was cooled to room temperature and diluted with 5 mL of deionized water. Next, the solution was filtered through a microporous membrane (0.22 μm) and dialyzer (MWCO 1000 Da) to obtain the Arg-CD solution and finally freeze-dried to obtain a brown powder.

Procedure for fluorescent determination of Arg-CD

The Arg-CD was dissolved in deionized water beforehand to prepare the stock solution (1 mg/ 1 mL) and was diluted to certain concentration with a PBS buffer (pH 7.4, 1.0 mM). Stock solutions (1.0 mM) of $ZnCl_2$ (Zn^{2+}), $AgNO_3$ (Ag^+), $CaCl_2$ (Ca^{2+}), $CuSO_4$ (Cu^{2+}), $Co(HAC)_2$ (Co^{2+}), $FeCl_2$ (Fe^{2+}), $FeCl_3$ (Fe^{3+}), $MgSO_4$ (Mg^{2+}), $Pd(HAC)_2$ (Pd^{2+}), $Na_2S_2O_3$ ($S_2O_3^{2-}$), $NaNO_2$ (NO_2^-),
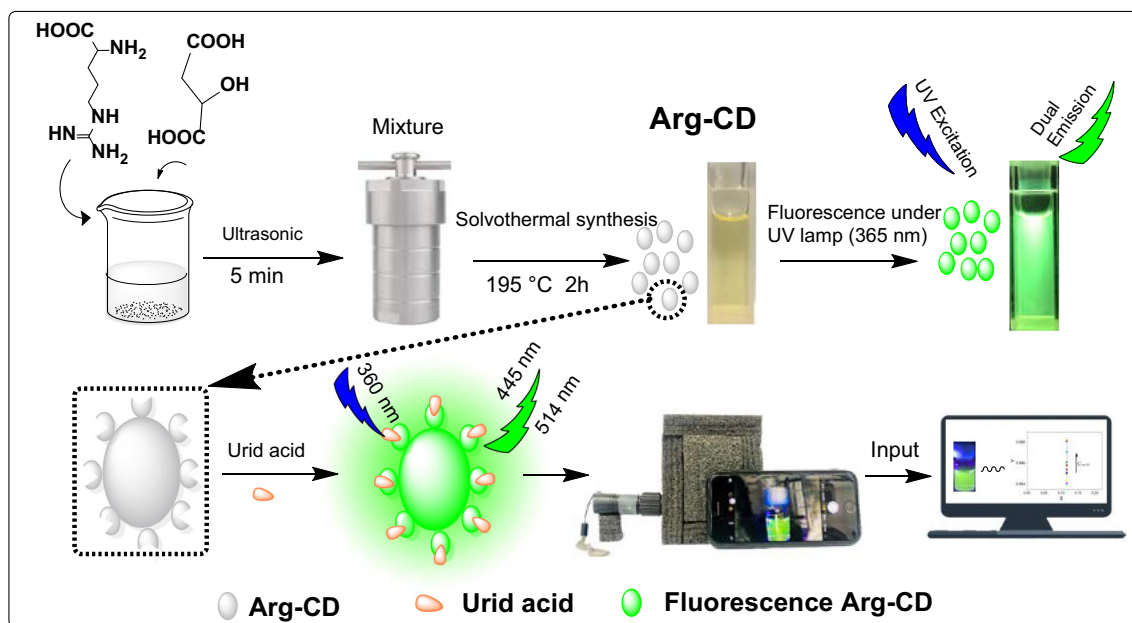
Scheme 1. Arg-CD synthesis strategy for UA determination and application in the miniaturized device.

NaHCO$_3$(HCO$_3^-$), L-arginine (Arg), L-aspartic acid (Asp), L-ascorbic acid (AA), L-cysteine (Cys), (Crn), L-tyrosine (Tyr), cadaverine (Cad), putrescine (Put), L-glutamine (Glu), glucose, sucrose, L-glycine (Gly), L-glutathione (GSH), L-histidine (His), urea, hydroquinone (HQ), melamine, L-phenylalanine (Phe), L-proline (Pro), streptomycin (SM), penicillin (PG), xanthine, adenine (Ade), caffeine, cholesterol (Chol), uridine 5′-triphosphate trisodium salt (UTP), sodium 3,5-cyclic adenosine monophosphate (CMP), cytidine-5′-triphosphate disodium salt (CTP), guanosine 5′-triphosphate trisodium salt (GTP), adenosine triphosphate (ATP), adenosine 5′-monophosphate (AMP), adenosine-5′-diphosphate (ADP), and uric acid (UA) were prepared in deionized water. All spectrum measurements were taken at room temperature and performed in the PBS buffer (pH 7.4, 1.0 mM).

To evaluate the sensitivity of Arg-CD (3 mg/20 mL) to UA, different concentrations of UA standard solution were in addition to the **Arg-CD** solution and adjusted to the required concentration (0.0–800 μM). To evaluate the selectivity of Arg-CD (3 mg/5 mL) to UA (0.42 mM), a series of analytes (1 mM) were tested, including Zn^{2+}, Ag$^+$, Ca^{2+}, Cu^{2+}, Co^{2+}, Fe^{2+}, Fe^{3+}, Mg^{2+}, Pd^{2+}, S$_2$O$_3^{2-}$, NO$_2^-$, HCO$_3^-$, Arg, Asp, AA, Cys, Crn, Tyr, Cad, Put, Glu, glucose, sucrose, Gly, GSH, His, urea, HQ, melamine, Phe, Pro, SM, PG, xanthine, Ade, caffeine, Chol, UTP, CMP, CTP, GTP, ATP, AMP, ADP, and UA. Each experiment was performed at room temperature and was repeated three times.

Human serum sample test

For real sample analysis, human serum samples were obtained from normal human blood serum samples donated by Shanghai Sixth People's Hospital. The samples of blood serum were diluted 10 times with a PBS buffer without other pretreatments. The experimental procedures were identical for the determination of UA in the PBS buffer. UA in human serum samples was determined by the standard addition method. In all fluorescence measurements, the excitation is 360 nm and the emission intensity collected is at 514 nm, which was used for quantification. Then, the analyses of the actual samples of UA were performed using the procedure in the section of the procedure for fluorescent determination of Arg-CD.

Results and discussion

Characteristics of Arg-CD

Morphology of Arg-CD was observed by transmission electron microscopy (TEM). As shown in Fig. 1a, Arg-CD is nearly spherical without apparent aggregation. Their diameters mainly distribute in the range

of 3–30 nm with a mean value of about 5.6 nm (inset of Fig. 1a). Most of the particles can be observed to have highly discernible crystalline structures with well-resolved lattice edges. The lattice fringes of Arg-CD with a spacing of ca.0.31 nm can be observed by the HRTEM inset images (Fig. 1b), confirming that the synthesized Arg-CDs were graphite [24].

The photoluminescence properties of C and N co-doped Arg-CD aqueous solution are shown in Fig. 1c; the maximum excitation wavelength of Arg-CD is at 360 nm, which contacted two maximum emission peaks at 445 nm and 514 nm, respectively. The emission peak at 445 nm is due to the various surface states containing both single—and double-bonded oxygen functional groups on the surface of carbon dots, and the emission peak at 514 nm is due to $n - \pi^*$ transition related to the C=O/C=N bond on the surface of carbon dots. The fluorescence properties of carbon dots are mainly related to the different interactions between emission centers and non-radiative transitions caused by distinct functional groups [25]. Arg-CD showed a bright green color fluorescence under a UV lamp (inset of Fig. 1c). When Arg-CD was added to UA, the position of the absorption band did not change, but the absorption intensity changed (Fig. S1). According to the International Commission on Illumination (CIE) 1931 chromaticity diagrams, the visible spectra can be read with the aid of the CIE chromaticity coordinate in a chromaticity diagram [26]. As shown in Fig. 1d, the CIE coordinates of the emitted green light were realized at (0.1177, 0.6512).

The spectral property of Arg-CD in an aqueous solution was investigated. With the wavelength of excitation shifted from 340 to 380 nm, the fluorescence wavelength and intensity exhibited evident variations (Fig. 1e). The maximum emission wavelength at around 514 nm and the strongest emission intensity appeared with excitation at 360 nm, which was determined as the optimal excitation wavelength. This excitation-dependent behavior may be explained by the effect of intrinsic electronic conjugate structures of Arg-CD [27].

In the system, different ratios (L-arginine/DL-malic acid) of carbon dots were synthesized according to the above synthesis method and their different fluorescence emission curves were obtained. According to Fig. 1f, it can be found that the emission wavelength varies irregularly along with the increasing ratio of L-arginine. When the nitrogen amount is too low, the L-arginine surface groups can react with fewer DL-malic acid compared to the available amount in the reaction, resulting in clustering or freeing of DL-malic acid which harms increasing the active site. On the contrary, when the nitrogen amount is too high, it leads to nitrogen accumulation [28]. After optimization, when the L-arginine and DL-malic acid ratio was 1.5:1 (Fig. 1f), the reaction temperature was 195 °C (Fig. S2A), the reaction solvent was water (Fig. S2B), the reaction time was 2 h (Fig. S2C), and the determination solvent was water (Fig. S2D), Arg-CD performed dual-emission peak at 445 nm and 514 nm with excitation at 360 nm. This characteristic means Arg-CD had good compatibility with the existing instruments. At the same time, the dual-emission spectrum can provide more data for internal correction.

## Fourier transform infrared (FTIR) spectroscopy of Arg-CD

To confirm the surface-bound interactions between Arg-CD and UA, Fourier transform infrared spectroscopy was recorded at 400–4000 cm^{-1}. Arg-CD shows similar characteristic absorption bands of DL-malic acid [29] and L-arginine [21], which reveal the existence of raw material-derived functional groups on the surface of the synthesized Arg-CD (Fig. S3). As shown in Fig. 2A, the absorption spectrum of—NH$_2$ tensile vibration at 420–505 cm^{-1} was found and the peaks at 1398 and 3180 cm^{-1} were due to N–H tensile vibration, which indicates the presence of amino groups on the nitrogen-doped Arg-CD surface. The peak at 1673 cm^{-1} was assigned to carbonyl group stretching or C=N stretching vibrations, while the peaks located at 3370 cm^{-1} were ascribed to O–H. With the vibration of the purine ring in UA [30], UA displayed a characteristic absorption band at 3009 cm^{-1} (Fig. 2b). The FTIR for Arg-CD and Arg-CD + UA revealed the existence of C–O stretching vibrations at 1046 and 947 cm^{-1}, implying that they had a similar skeletal structure. FTIR confirmed the successful incorporation of a nitrogen atom into the carbon structures, and a large amount of carboxyl, hydroxyl, and amino groups on the surface of the Arg-CD could improve its stability and hydrophilicity.
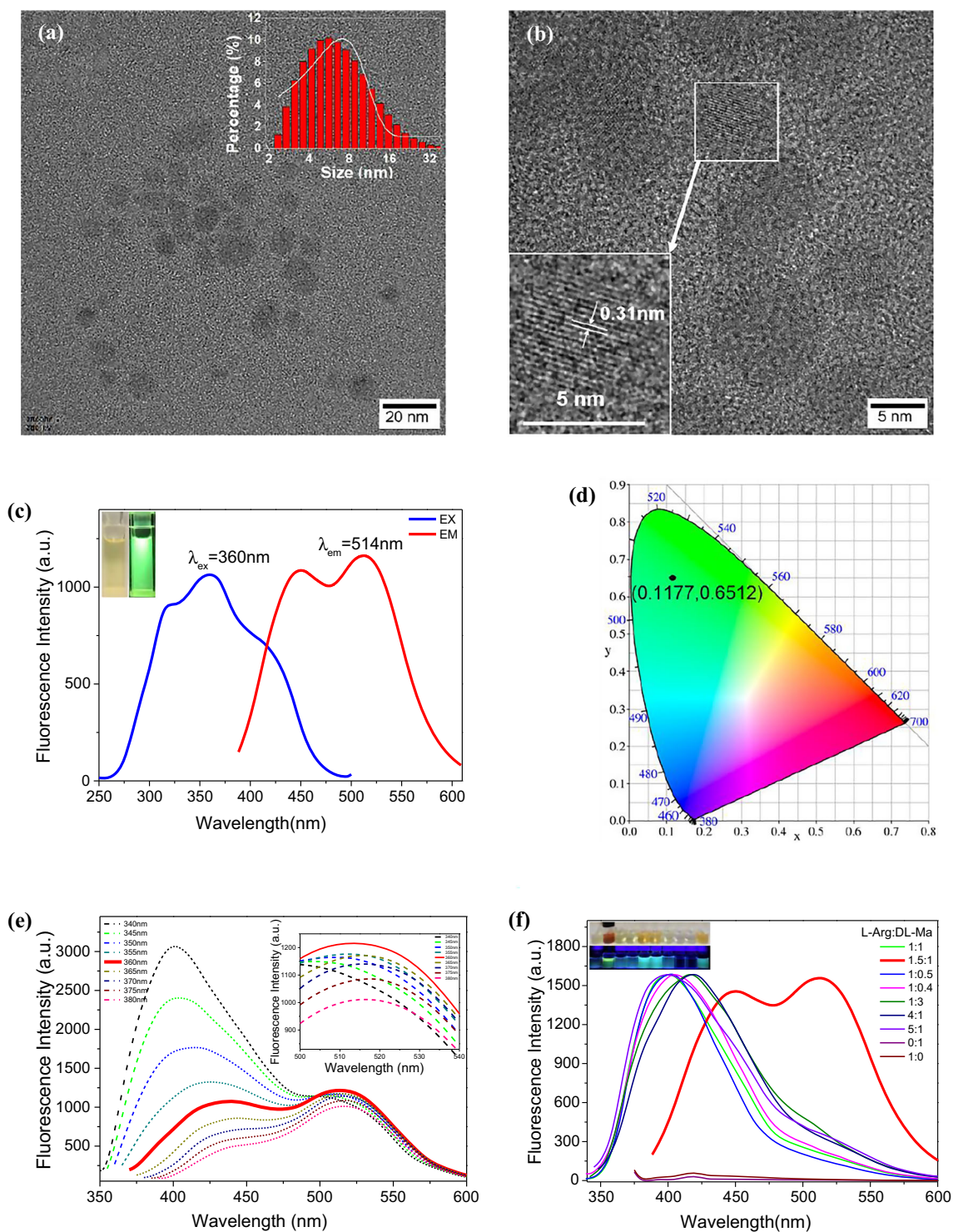
Figure 1 **a** Arg-CD TEM image with a scale bar of 20 nm, inset: particle size distribution of Arg-CD; **b** Arg-CD TEM image with a scale bar of 5 nm, inset: HRTEM image; **c** fluorescence excitation spectrum (blue line) and emission spectrum (red line) of Arg-CD (1 mg/1 mL), inset: Arg-CD photographs under sunlight and 365 nm UV light; **d** CIE 1931 chromaticity diagram of Arg-CD; **e** fluorescence emission spectra of Arg-CD (1 mg/1 mL) at different excitation wavelengths; **f** fluorescence spectra of Arg-CD (3 mg/2 mL) with different ratios (L-arginine/DL-malic acid), inset: Arg-CD photographs at different ratios under sunlight and 365 nm UV light. ($\lambda_{ex} = 360$ nm).

Figure 2 **a** FTIR of Arg-CD; **b** FTIR of Arg-CD and UA and their mixture; **c** full-range XPS spectrum of Arg-CD; **d** high-resolution C_{1s} XPS spectrum; **e** high-resolution N_{1s} XPS spectrum; **f** high-resolution O_{1s} XPS spectrum.
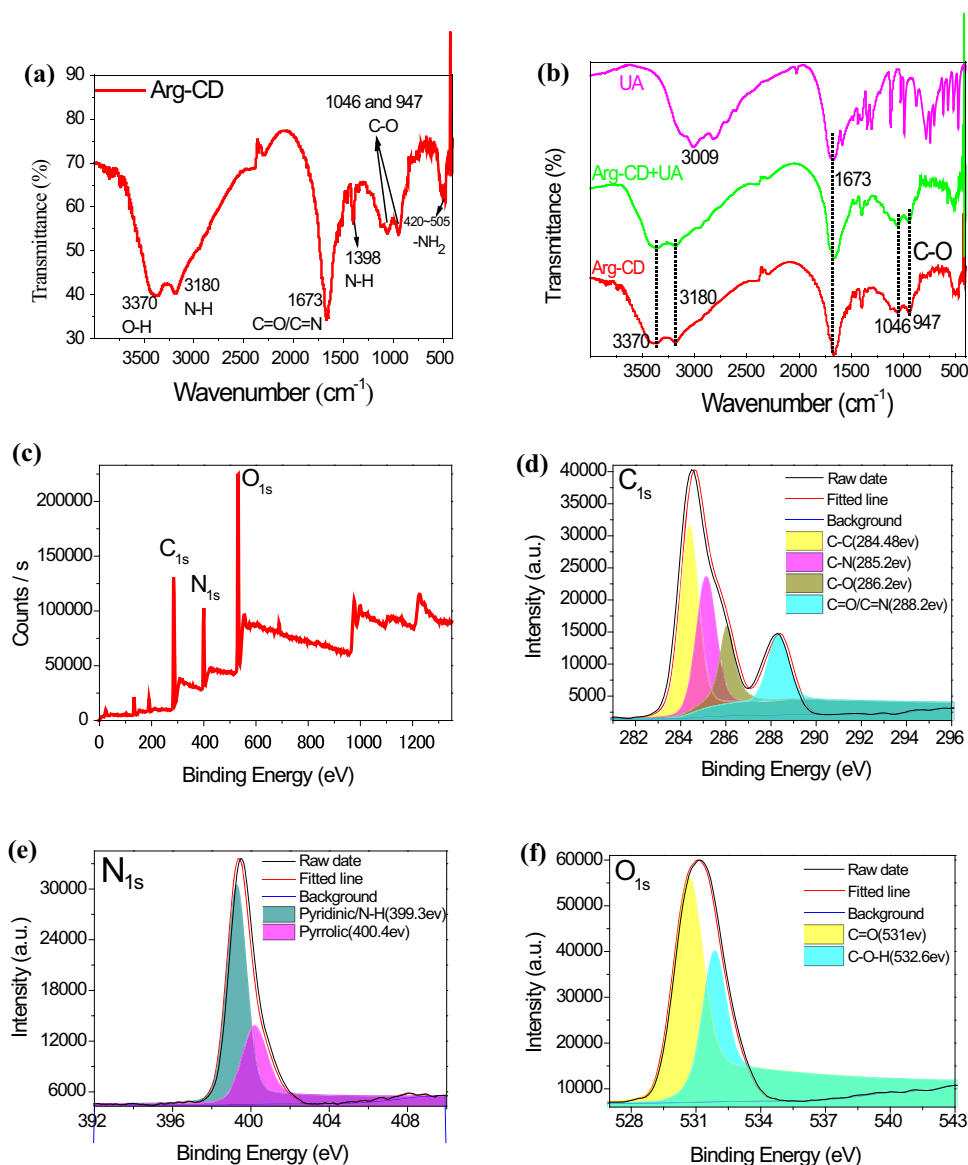
X-ray photoelectron spectroscopy (XPS) of Arg-CD

XPS is considered a powerful tool for determining surface-bound interactions and surface purity in hybrid nanomaterials, which was used to further study the surface element analysis and functional groups of Arg-CD [31]. The XPS full-scan spectra exhibited the presence of peaks for carbon, nitrogen, and oxygen which was also in line with the results of elemental analysis (Fig. 2c). After aligned and corrected nuclear-level binding energy using carbon (1 s), the peaks of good-resolution binding energy for O_{1s}, N_{1s}, and C_{1s} were found to be located at 531.1, 399.6, and 284.6 eV, respectively. The C_{1s} spectrum could be consisting of four peaks located at 284.48, 285.2, 286.2, and 288.2 eV indicating C–C, C–N, C–O, and C=O/C=N bonds, respectively (Fig. 2d). The N_{1s} spectrum with the better-resolved peaks located at 399.3 and 400.4 eV was attributed to pyridine (C–N–C)/N–H and pyrrole (C_2–N–H), respectively (Fig. 2e). The peaks of the O_{1s} spectrum at 531.0 and 532.6 eV were corresponded to C=O and C–O–H, respectively (Fig. 2f). The atomic percentages of C, N, and O were found to be 52.24%, 18.06%, and 29.7%, respectively. The results of XPS showed that the surface of Arg-CD had various functional groups such as C–N, C=O, N–H, C=O, and C_2–N–H. From the above, we could conclude that a new type of Arg-CD has been successfully synthesized [32].

Stability of Arg-CD

To further evaluate the stability of Arg-CD, the effects of time, temperature, pH value, and salt solutions on the fluorescence intensity of both Arg-CD and Arg-CD + UA were investigated.

The fluorescence intensity of Arg-CD and Arg-CD + UA remained stable after UV irradiation for about 1 min (Fig. S4A–B), 10 min (Fig. S4C–D), and 450 min (Fig. S4E–F). In the range of 30–75 °C, fluorescence is still maintained (Fig. S5A–B), and the fluorescence intensity of both samples remained stable in pH value from 5.0 to 10.0 (Fig. S5C–D). Even in Na^+ (0–200 mM) and K^+ (0–7 mM) solutions, the fluorescence intensity of **Arg-CD** remained almost constant (Fig. S6A–D). Therefore, Arg-CD displayed good stability time, temperature, pH, and salt solutions, which provide a good assurance for biological application.

Fluorescence determination of UA

The reactivity of Arg-CD toward UA was performed in the PBS buffer (pH 7.4, 1.0 mM) at room temperature. Without UA, the fluorescent intensity of Arg-CD was weak with excitation at 360 nm. Upon addition of UA, the Arg-CD showed dual-emission fluorescence enhancement at 445 nm and 514 nm (Fig. 3a) and stabilized within 1 min (Fig. S7). The kinetics data of Arg-CD were collected in the presence of UA (100 μM) and emission at 514 nm. These results showed that the Arg-CD has the potential for real-time determination for UA.

The fluorescence response between Arg-CD and the concentrations of UA was studied with emission at 445 nm and 514 nm (Fig. 3b). Fluorescence response of Arg-CD to UA displayed a good regularity in the range of 20–800 μM and can be expressed by $F_{445} + F_{514} = -8482.6\ C^2 + 11{,}457.2\ C + 668.7$ with the coefficient of determination (R^2) of 0.99, where C refers to the concentration of UA. However, there was excellent linearity in the physiological range (330 ∼ 630 μM), satisfying the equation $F_{445} + F_{514} = 3250.5\ C + 2509.6$ with the coefficient of determination (R^2) of 0.974 (inset of Fig. 3b). And the limit of detection (LOD) is estimated to be 7.14 μM (Eq. S1).

The synthesized Arg-CD also kept the dual fluorescent emission when combined with UA. With the concentration of UA increase, we could find an obvious fluorescent intensity increase from 430 to 535 nm which performs a dual emission. In this range, about 105 nm, the amplitude of the signal strength is almost the same, which means that we can collect signals arbitrarily in the wavelength of 430–535 nm and maintain high accuracy (Fig. 3c). This is very important for us to collect signals through mobile phones in the next experiment. A comparison between this carbon dot and other reported carbon dots for UA determination is summarized in Table S1, which showed that the **Arg-CD** has a faster response time than most of the reported probes. These results reported that the Arg-CD could sensitively and rapidly detect UA under physiological conditions.

To investigate the mechanism, UV–Vis absorption spectra from Arg-CD, Arg-CD + UA, and UA (Fig. S1) observed that UA has no absorption within 300–600 nm [33], and Arg-CD absorption increases in the presence of UA without blue- or redshift, which may be due to the interaction with Arg-CD and UA [34]. The similarity of Arg-CD and Arg-CD + UA structures was also revealed, which was also confirmed by FTIR spectroscopy [35]. According to the exponential function $Y(t)$ fitting formula (Eq. S2), the average fluorescence lifetime of Arg-CD is 10.98 ns and that of Arg-CD + UA is 11.18 ns (Fig. 4a), which indicates that the lifetime value does not change markedly [36, 37]. As shown in Fig. 4b, there is almost no overlap between the UV absorption spectrum of UA and the emission spectrum of Arg-CD, which indicates that there is no effective inner filter effect or Förster resonance energy transfer between Arg-CD and UA [38].

The observational results show that FTIR and XPS confirmed the presence of carboxyl, hydroxyl, and amino groups on the surface of Arg-CD. As shown in Fig. 4c, the zeta potential of Arg-CD was + 4.09 mV, indicating a positive charge on the surface of Arg-CD, which was related to the presence of the amino group on the surface of Arg-CD. And the zeta potential of Arg-CD changed to − 5.76 mV after the addition of UA, which was due to the action of UA on the outer surface of Arg-CD [34]. Under weakly alkaline conditions, the carboxyl group of Arg-CD is negatively charged, while the secondary amine group in the UA molecule is positively charged, and there is an electrostatic interaction between them [39] and changes the distance between them [40]. Uric acid is a dibasic acid that, at a biological pH, forms a single charged
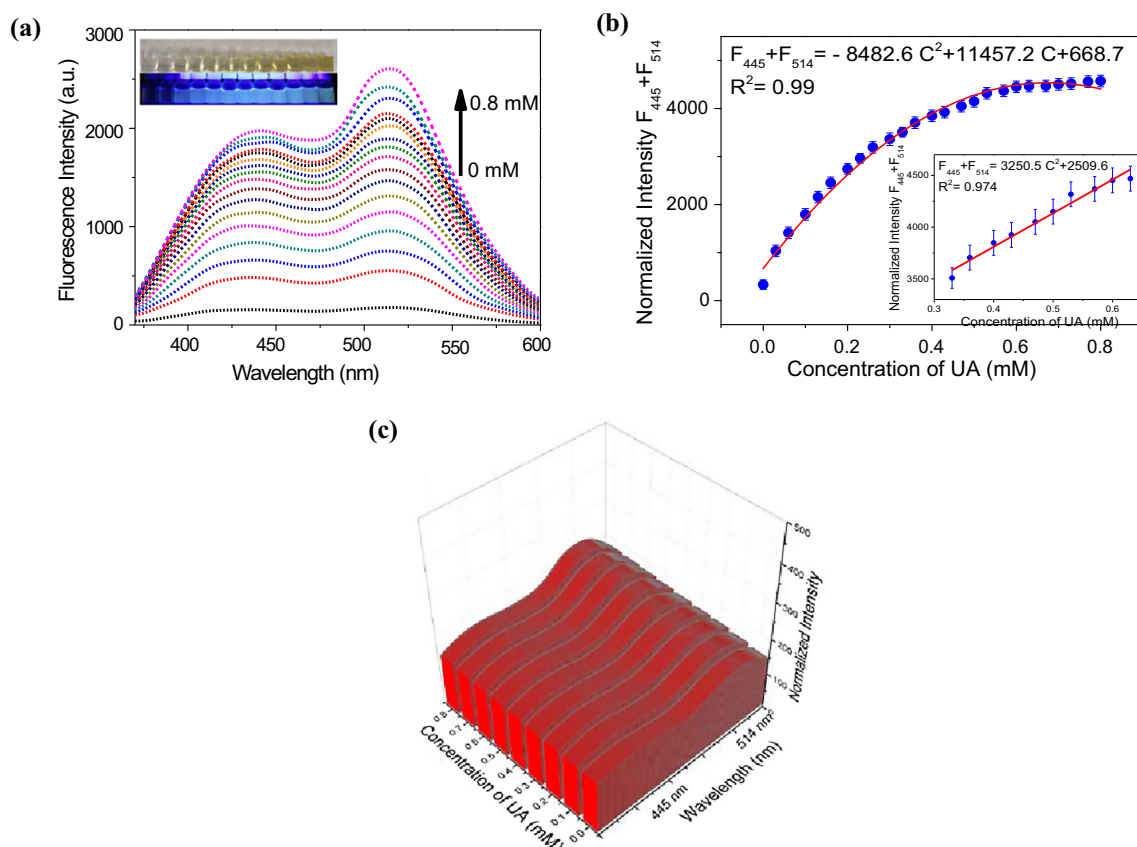
Figure 3 **a** Fluorescence titration curve of Arg-CD (3 mg/20 mL) with different concentrations of UA from 0.0 to 0.8 mM; **b** regular relationship between fluorescence factor $F_{445} + F_{514}$ and the concentration of uric acid at 445 nm and 514 nm, inset: corresponding linear fitting curve; **c** a three-dimensional histogram of the normalized intensity. ($\lambda_{ex} = 360$ nm). F_{445} represents the fluorescence intensity of Arg-CD in 445 nm; F_{514} represents the fluorescence intensity of Arg-CD in 514 nm.

hydrogen or acid urate ion, is deprotonated on nitrogen atom, and uses a tautomeric ketone/hydroxyl group as an electron-absorbing group, the formation of hydrogen bonds between the ketone/hydroxyl group in the UA molecule and the amino group on the surface of Arg-CD [41], the compression of the electron wave function in the dot, leading to an increase in the degree of electron localization and an increase in the surface defects of Arg-CD [33], resulting in enhanced fluorescence. As shown in Fig. 4d, when UA is added, UA acts on the surface of Arg-CD to increase the particle size. Under weak alkaline conditions, UA is better dispersed, which promotes the maximum response of Arg-CD to UA [39, 41].

## Selectivity of Arg-CD toward other related substances

To study the selectivity of Arg-CD toward UA, the fluorescence response of the Arg-CD was studied in the presence of various substances at 445 nm and 514 nm, including Zn^{2+}, Ag^+, Ca^{2+}, Cu^{2+}, Co^{2+}, Fe^{2+}, Fe^{3+}, Mg^{2+}, Pd^{2+}, $S_2O_3^{2-}$, NO_2^-, HCO_3^-, Arg, Asp, AA, Cys, Crn, Tyr, Cad, Put, Glu, glucose, sucrose, Gly, GSH, His, urea, HQ, melamine, Phe, Pro, SM, PG, xanthine, Ade, caffeine, Chol, UTP, CMP, CTP, GTP, ATP, AMP, ADP, and UA in the PBS buffer (Fig. 5a). In the presence of UA, Arg-CD displayed remarkable fluorescence enhancement. On the contrary, other substances introduced nearly no fluorescent changes. Selectivity normalization intensity of these interfering substances is much lower than UA (Fig. 5b), indicating that the degree of change in the system fluorescence intensity caused by these interfering substances is negligible. Compared to the

(a)

(b)

(c)

(d)
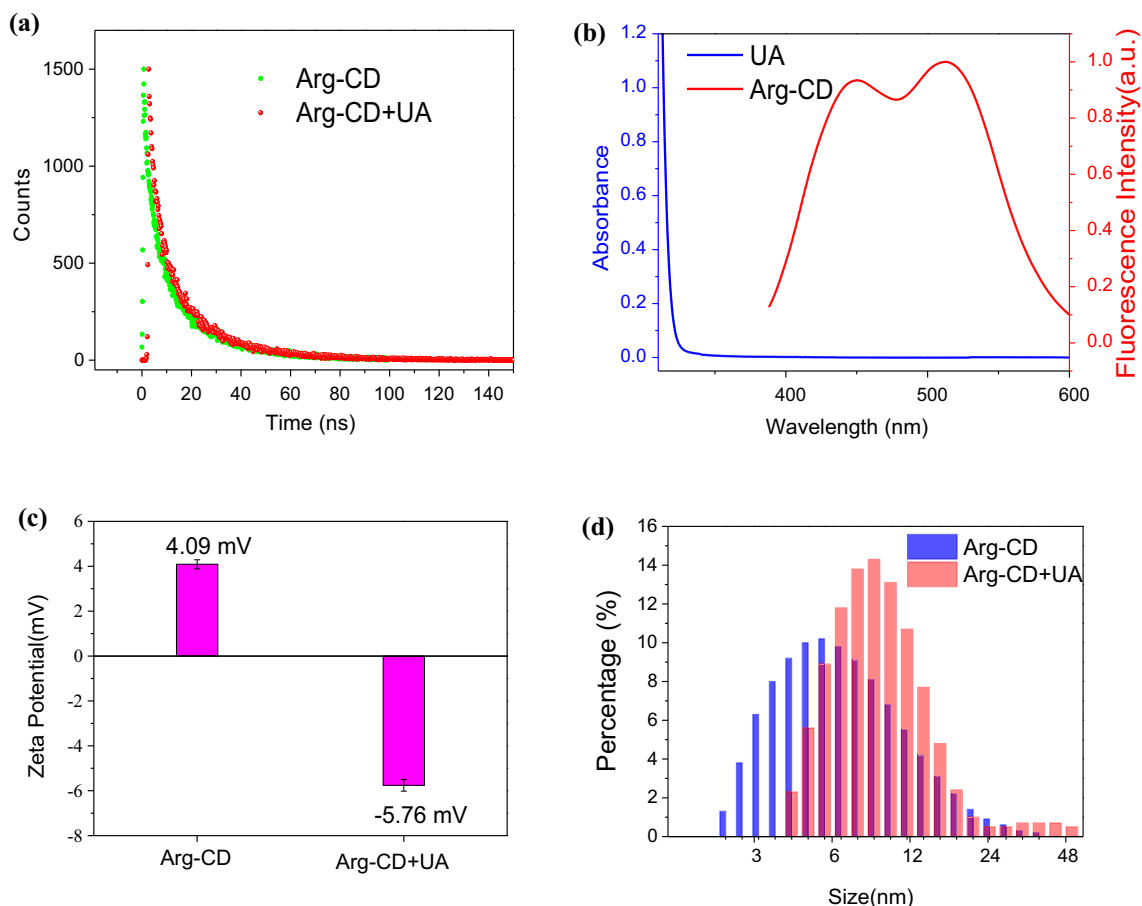
Figure 4 a Fluorescence decay curves of Arg-CD (1 mg/1 mL) and Arg-CD + UA; **b** UV–Vis spectra of UA (1 mM) plotted against fluorescence emission spectra of Arg-CD (1 mg/1 mL) (λ_{ex} = 360 nm); **c** zeta potential diagram of Arg-CD and Arg-CD + UA; **d** particle size distribution of Arg-CD and Arg-CD + UA.

(a)

(b)
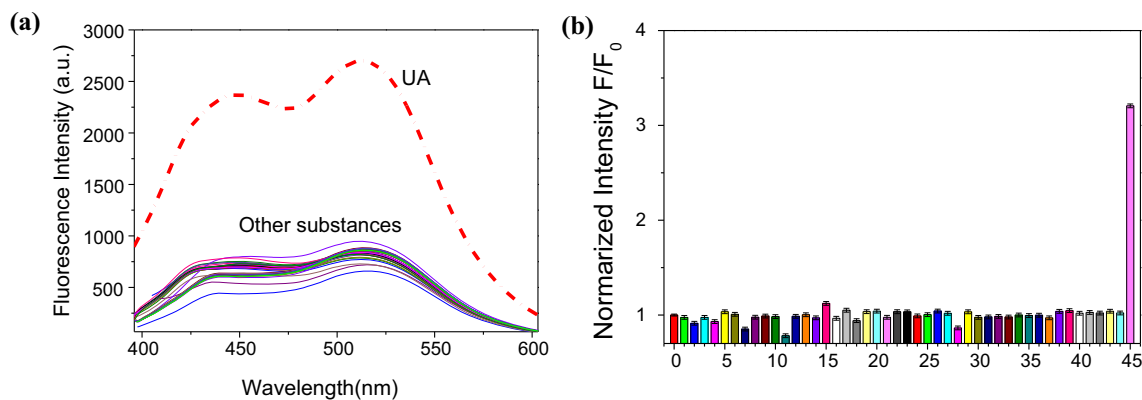
Figure 5 a Fluorescence emission spectrum changes of Arg-CD (3 mg/5 mL) + UA (0.42 mM) mixed with all substances; **b** the selectivity normalization intensity of Arg-CD + UA with interference substances at 514 nm. (0: Blank, 1: Zn^{2+}, 2: Ag^+, 3: Ca^{2+}, 4: Cu^{2+}, 5: Co^{2+}, 6: Fe^{2+}, 7: Fe^{3+}, 8: Mg^{2+}, 9: Pd^{2+}, 10: $S_2O_3^{2-}$, 11: NO_2^-, 12: HCO_3^-, 13: Arg, 14: Asp, 15: AA, 16: Cys, 17: Crn, 18: Tyr, 19: Cad, 20: Put, 21: Glu, 22: glucose, 23: sucrose, 24: Gly, 25: GSH, 26: His, 27: Urea, 28: HQ, 29: melamine, 30: Phe, 31: Pro, 32: SM, 33: PG, 34: xanthine, 35: Ade, 36: caffeine, 37: Chol, 38: UTP, 39: CMP, 40: CTP, 41: GTP, 42: ATP, 43: AMP, 44: ADP, 45: UA). F_0 represents the original fluorescence intensity of Arg-CD; F represents the fluorescence intensity of Arg-CD with different substances, λ_{ex} = 360 nm.

blank sample (Fig. S8A–D), the relative fluorescence intensity F/F_0 in the presence of UA was unaffected by the interfering substances, suggesting that the interference of the coexisted UA was negligible. These results demonstrated that Arg-CD with the high selectivity toward UA determination could be an ideal photoluminescence sensor for UA.

Application of Arg-CD in human serum samples

To evaluate the practicability of the proposed carbon dot on actual samples, the preparation method was applied to determine the concentration of uric acid in nine human serum samples. For example, the habitual level of uric acid in the serum for healthy people is 240–520 μM. We used an automated biochemistry analyzer to measure nine freshly obtained serum samples.

As shown in Fig. 6, a linear relationship exists between the Arg-CD normalized standard concentration and the results obtained from the automatic biochemical analyzer. The linear regression equation is $Y = X + 2.2$ with a coefficient of determination (R^2) of 0.998.

The results of the analysis are shown in Table 1. The accuracy rate of uric acid in nine human serum samples is in the range of 98.5–101.5%, and the relative standard deviations (RSD) of the three repeated measurements are all lower than 4%, suggesting the excellent repeatability of this method. These results
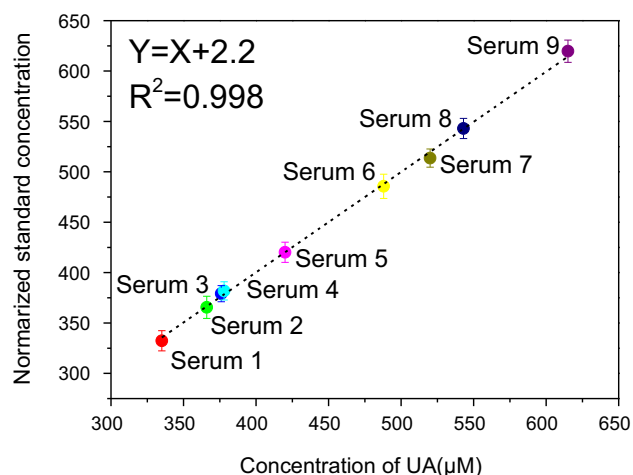
Figure 6 Correlation curves between Arg-CD sensing signals and biochemical analyzers for human serum samples. *X* represents the biochemical analyzer results, and *Y* represents the Arg-CD sensing signal.

indicate that the Arg-CD could be used for UA determination in human real samples. Therefore, the results summarized in Table 1 further demonstrated the practical value of this method for uric acid determination in human serum.

Checking Arg-CD luminosity with a UV flashlight

A self-made dark box, a cell phone, and a UV flashlight were used as miniaturized devices. As shown in Fig. S9, the pictures of Arg-CD solutions with different concentrations were visible under sunlight, UV analyzer (365 nm), and UV flashlight. Being compared to the UV analyzer, the fluorescent signals were much brighter when irradiated by the UV flashlight. The photographic images were digitally processed and mapped to the CIE 1931 *XY* chromaticity diagram [42]. Here, we found that the fluorescence variation luminosity of Arg-CD could be analyzed using the *Y* part of the CIE 1931 *XY* color space. We used an inexpensive miniaturized UV flashlight to replace the traditional UV analyzer for rapid fluorescent determination, which verified the feasibility of utilizing Arg-CD to detect UA by visual fluorescence changes in daily life.

Conclusions

In summary, arginine–malate-based dual-emission carbon dots using L-arginine and DL-malic acid as precursors were prepared by a simple and rapid solvothermal synthesis method. Due to the substitution of non-metallic *N* elements, Arg-CD exhibits excellent photochemical properties. After mixing with UA, an obvious fluorescent intensity is enhanced from 430 to 535 nm and the amplitude of the signal strength is almost the same. Under the physical conditions, fluorescence signal and uric acid concentration had a very good regularity at 445 nm and 514 nm and the coefficient of determination (R^2) was 0.99 and 0.974. Probe Arg-CD also performed high selectivity of uric acid to other potential interfering substances. The human serum experiment proved that Arg-CD showed similar accuracy to current clinical testing methods. The accuracy rate of uric acid in nine human serum samples is in the range of 98.5–101.5%, and the RSD measurements are all lower than 4%. Meanwhile, we designed a simple,

Table 1 The results of UA determination in human serum samples

Sample	Biochemistry analyzer (μM)	RSD (%, $n = 3$)	Found (μM)	Accuracy (%)
Serum 1	335	1.45	332.38	99.21
Serum 2	366	1.88	365.57	99.88
Serum 3	376	1.84	379.14	100.84
Serum 4	378	1.35	381.85	101.02
Serum 5	420	1.87	420.20	100.05
Serum 6	488	2.23	485.64	99.52
Serum 7	520	3.93	513.65	98.78
Serum 8	543	2.22	543.02	100.00
Serum 9	615	1.19	619.70	100.77

low-cost miniaturized device that could realize convenient and fast UA determination. The relevant APP is in preparation, and then the speedy determination of uric acid can be realized through the mobile phone.

Declarations

Conflict of interest The authors declare that they have no conflict of interest.

Supplementary Information: The online version contains supplementary material available at https://doi.org/10.1007/s10853-021-06660-0.

References

[1] Zhao L, Blackburn J, Brosseau CL (2015) Quantitative detection of uric acid by electrochemical-surface enhanced raman spectroscopy using a multilayered Au/Ag substrate. Anal Chem 87:441–447

[2] Xiong Q, Liu V, Xu YC (2019) Effects of uric acid on diabetes mellitus and its chronic complications. Int J Endocrinol 2019:1–8

[3] Watanabe S, Kawano T, Horino T, Matsumoto T, Nagata K, Hatakeyama Y, Locatelli FM, Yokoyama M, Terada Y, Okuhara Y (2019) Influence of hyperuricemia treatment on postoperative acute kidney injury among hyperuricemia patients: a single-center retrospective database analysis. BMC Res Notes 12:1–5

[4] Simonato M, Agoston DV, Brooks KA, Dulla C, Fureman B, Henshall DC, Pitkänen A, Theodore WH, Twyman RE, Kobeissy FH, Wang KK, Whittemore V, Wilcox KS (2021) Identification of clinically relevant biomarkers of epileptogenesis: a strategic roadmap. Nat Rev Neurol 17:231–242

[5] Zhu J, Chu HY, Shen JW, Wang CZ, Wei YM (2021) Nitrogen and fluorine co-doped green fluorescence carbon dots as a label-free probe for determination of cytochrome c in serum and temperature sensing. J Coll Interface Sci 586:683–691

[6] Sha R, Vishnu N, Badhulika S (2019) MoS$_2$ based ultra-low-cost, flexible, non-enzymatic and non-invasive electrochemical sensor for highly selective detection of uric acid in human urine samples. Sens Actuators B Chem 279:53–60

[7] Hinterberger V, Damm C, Haines P, Guldi DM, Peukert W (2019) Purification and structural elucidation of carbon dots by column chromatography. Nanoscale 11:8464–8474

[8] Maleki S, Madrakian T, Afkhami A (2018) Application of polyacrylonitrile nanofibers decorated with magnetic carbon dots as a resonance light scattering sensor to determine famotidine. Talanta 181:286–295

[9] Xie X, Wang DP, Guo CX, Liu YH, Rao QH, Lou FM, Li QN, Dong YQ, Li QF, Yang HB, Hu FX (2021) Single-atom ruthenium biomimetic enzyme for simultaneous electrochemical detection of dopamine and uric acid. Anal Chem 93:4916–4923

[10] Shi B, Su YB, Duan Y, Chen SY, Zuo WY (2019) A nanocomposite prepared from copper(II) and nitrogen-doped graphene quantum dots with peroxidase mimicking properties for chemiluminescent determination of uric acid. Microchim Acta 186:1–10

[11] Wang Q, Wen X, Kong JM (2019) Recent progress on uric acid detection: a review. Crit Rev Anal Chem 50:359–375

[12] Guo R, Li L, Wang BW, Xiang YE, Zou GQ, Zhu YR, Hou HS, Ji XB (2021) Functionalized carbon dots for advanced batteries. Energy Storage Mater 37:8–39

[13] Zhang HQ, Wang H, Wang Y, Xin BF (2020) Controlled synthesis and photocatalytic performance of biocompatible

uniform carbon quantum dots with microwave absorption capacity. Appl Surf Sci 512:145751

[14] Miao S, Liang K, Zhu JJ, Yang B, Zhao DY, Kong B (2020) Hetero-atom-doped carbon dots: doping strategies, properties and applications. Nano Today 33:100879

[15] Hoang V, Dave K, Gomes VG (2019) Carbon quantum dot-based composites for energy storage and electrocatalysis: mechanism, applications and future prospects. Nano Energy 66:104093

[16] Kalaiyarasan G, Veerapandian M, JebaMercy G, Balamurugan K, Joseph J (2019) Amygdalin-functionalized carbon quantum dots for probing β-glucosidase activity for cancer diagnosis and therapeutics. ACS Biomater Sci Eng 5:3089–3099

[17] Pardo J, Peng ZL, Leblanc RM (2018) Cancer targeting and drug delivery using carbon-based quantum dots and nanotubes. Molecules 23:378

[18] Wu P, Xu YX, Zhan JY, Li Y, Xue HG, Pang H (2018) The research development of quantum dots in electrochemical energy storage. Small 14:1801479

[19] Han Y, Yang WX, Luo XL, He X, Yu Y, Li CH, Tang WZ, Yue TL, Li ZH (2019) Cu^{2+}-triggered carbon dots with synchronous response of dual emission for ultrasensitive ratiometric fluorescence determination of thiophanate-methyl residues. J Agric Food Chem 67:12576–12583

[20] Hou J, Li H, Tang YQ, Sun JY, Fu H, Qu X, Zheng S (2018) Supported N-doped carbon quantum dots as the highly effective peroxydisulfate catalysts for bisphenol F degradation. Appl Catal B 238:225–235

[21] Fu C, Qian K, Fu AL (2017) Arginine-modified carbon dots probe for live cell imaging and sensing by increasing cellular uptake efficiency. Mater Sci Eng C 76:350–355

[22] Zhao D, Ma WT, Xiao XC (2018) The recognition of sweat latent fingerprints with green-emitting carbon dots. Nanomaterials 8:612

[23] Pang S, Zhang Y, Wu CK, Feng SL (2016) Fluorescent carbon dots sensor for highly sensitive detection of guanine. Sens Actuators B Chem 222:857–863

[24] Atchudan R, Edison T, Sethuraman MG, Lee YR (2016) Efficient synthesis of highly fluorescent nitrogen-doped carbon dots for cell imaging using unripe fruit extract of prunus mume. Appl Surf Sci 384:432–441

[25] Mohan R, Drbohlavova J, Hubalek J (2018) Dual band emission in carbon dots. Chem Phys Lett 692:196–201

[26] Liu R, Yang R, Qu CJ, Mao HC, Hu Y, Li JJ, Qu LB (2017) Synthesis of glycine-functionalized graphene quantum dots as highly sensitive and selective fluorescent sensor of ascorbic acid in human serum. Sens Actuators B Chem 241:644–651

[27] Yang S, Wang K, Wang X, Sun XH (2020) Organic acid participation strategy for the synthesis of highly fluorescent carbon dots and their application in dual-mode determination of copper ions. Appl Surf Sci 505:144567

[28] Sudolská M, Otyepka M (2017) Exact roles of individual chemical forms of nitrogen in the photoluminescent properties of nitrogen-doped carbon dots. Appl Mater Today 7:190–200

[29] Kumar N, Gupta SK, Jagadeesh D, Kanny K, Bux F (2015) Development of poly (aspartic acid-co-malic acid) composites for calcium carbonate and sulphate scale inhibition. Environ Technol 36:1281–1290

[30] Durán G, Benavidez TE, Contento AM, Ríos A, García CD (2017) Analysis of penicillamine using Cu-modified graphene quantum dots synthesized from uric acid as single precursor. J Pharm Anal 7:324–331

[31] Lu W, Gao YF, Jiao Y, Shuang SM, Li CZ, Dong C (2017) Carbon nano-dots as a fluorescent and colorimetric dual-readout probe for the detection of arginine and Cu(2+) and its logic gate operation. Nanoscale 9:11545–11552

[32] Yang P, Zhu ZQ, Zhang T, Zhang W, Chen WM, Cao YZ, Chen MZ, Zhou XY (2019) Orange-emissive carbon quantum dots: toward application in wound pH monitoring based on colorimetric and fluorescent changing. Small 15:1902823

[33] Zhang T, Sun XY, Liu B (2011) Synthesis of positively charged CdTe quantum dots and detection for uric acid. Spectrochim Acta Part A 79:1566–1572

[34] Sahoo N, Jana GC, Aktara MN, Das S, Nayim S, Patra A, Bhattacharjee P, Bhadra K, Hossain M (2020) Carbon dots derived from lychee waste: Application for Fe(3+) ions sensing in real water and multicolor cell imaging of skin melanoma cells. Mater Sci Eng C Mater Biol Appl 108:110429

[35] Zhou Y, Liyanage PY, Geleroff DL, Peng ZL, Mintz KJ, Hettiarachchi SD, Pandey RR, Chusuei CC, Blackwelder PL, Leblanc RM (2018) Photoluminescent carbon dots: a mixture of heterogeneous fractions. ChemPhysChem 19:2589–2597

[36] Huang S, Yang E, Yao J, Chu X, Liu Y, Zhang Y, Xiao Q (2019) Nitrogen, cobalt co-doped fluorescent magnetic carbon dots as ratiometric fluorescent probes for cholesterol and uric acid in human blood serum. ACS Omega 4:9333–9342

[37] Li C, Zheng YK, Ding HW, Jiang H, Wang XM (2009) Chromium (III)-doped carbon dots: fluorometric detection of p-nitrophenol via inner filter effect quenching. Microchim Acta 186:1–8

[38] Liu H, Xu CY, Bai YL, Liu L, Liao DM, Liang JG, Liu LZ, Han HY (2017) Interaction between fluorescein isothiocyanate and carbon dots: Inner filter effect and fluorescence

resonance energy transfer. Spectrochim Acta Part A 171:311–316

[39] Chen Q, Zhu PP, Xiong J, Gao LX, Tan KJ (2019) A sensitive and selective triple-channel optical assay based on red-emissive carbon dots for the determination of PFOS. Microchem J 145:388–396

[40] Yang Y, Huo DQ, Wu HX, Wang XF, Yang JS, Bian MH, Ma Y, Hou CJ (2018) N, P-doped carbon quantum dots as a fluorescent sensing platform for carbendazim detection based on fluorescence resonance energy transfer. Sens Actuators, B Chem 274:296–303

[41] Zhao C, Jiao Y, Hu F, Yang YL (2018) Green synthesis of carbon dots from pork and application as nanosensors for uric acid detection. Spectrochim Acta Part A 190:360–367

[42] Liang T, Yang PW, Wu TH, Shi MH, Xu XY, Qiang TT, Sun XL (2020) A general strategy to quantify analytes through fluorescence chromaticity and luminosity. Chin Chem Lett 31:2975–2979

Publisher's Note Springer Nature remains neutral with regard to jurisdictional claims in published maps and institutional affiliations.